Water Research 204 (2021) 117600

Contents lists available at ScienceDirect

Water Research

journal homepage: www.elsevier.com/locate/watres

Insights into the electro-hybrid ozonation-coagulation process–Significance of connection configurations and electrode types

Xin Jin [a,b], Xinyue Xie [b], Shaohua Zhang [b], Chao Yang [b], Lu Xu [a], Xuan Shi [a], Pengkang Jin [a,b,*], Xiaochang C. Wang [b]

[a] School of Human Settlements and Civil Engineering, Xi'an Jiaotong University, Xi'an, Shaanxi Province 710049, China
[b] School of Environmental and Municipal Engineering, Xi'an University of Architecture and Technology, Xi'an, Shaanxi Province 710055, China

ARTICLE INFO

Keywords:
Electrocoagulation
Ozonation
Bipolar connection
Dual-coagulants
Hydrolyzed species

ABSTRACT

The electro-hybrid ozonation-coagulation process (E-HOC) integrates electrocoagulation (EC) and ozonation simultaneously in a single unit. Nevertheless, the performance of the EC process is highly dependent on the polar connection configuration (monopolar vs. bipolar connection) and the type of generated coagulants (single-coagulant vs. dual-coagulants). In this study, the removal efficiency of the E-HOC process with different connection configurations and types of coagulants was assessed. The E-HOC process with bipolar connection (BE-HOC) exhibited higher removal efficiency for wastewater treatment plant (WWTP) effluent organic matter and ibuprofen (IBP) compared with the E-HOC process with monopolar connection (ME-HOC). Furthermore, dual-coagulant generation (released from both Al and Fe electrodes) in the BE-HOC process greatly improved the WWTP effluent organic matter and IBP removal efficiency. Lower energy consumption was observed for the BE-HOC process compared with the ME-HOC process. It was found that ozonation promoted the polymerization reactions during coagulant hydrolyzis in the E-HOC process. Compared with the ME-HOC process, the BE-HOC configuration and dual-coagulant mode further facilitated polymeric hydrolyzed coagulant species formation, thereby improving ozone catalytic and coagulation performance. According to trapping experiments and EPR analysis, •OH formation was enhanced in the BE-HOC process and dual-coagulant mode. In addition, more active reaction sites of generated hydrolyzed coagulant species were observed with bipolar connection and in the dual-coagulant generation mode based on X-ray photoelectron spectroscopy (XPS) analysis.

1. Introduction

Electrocoagulation (EC) is a water and wastewater treatment technology that produces metal coagulant in situ by electrochemically dissolving sacrificial electrodes submerged in contaminated water (Ingelsson et al., 2020). EC has shown promise as an alternative treatment process to conventional chemical coagulation for certain drinking water (Heffron et al., 2019), municipal (Bicudo et al., 2021) and industrial wastewater (Ghahrchi et al., 2021) treatment applications. However, the EC process does not effectively destroy some resistant pollutants (Ghahrchi and Rezaee 2020). Therefore, the use of the EC process as a sole treatment process faces serious practical limitations, especially when the wastewater is highly polluted (Al-Qodah et al., 2020; Ghahrchi and Rezaee 2020). The performance of EC can be greatly enhanced by coupling it with other treatment processes.

Previous studies have reported that EC can be synergistically coupled with other treatment processes, including electrocoagulation-ozonation processes, electrocoagulation-adsorption processes, electrocoagulation-ultrasound processes and electrocoagulation-pulses processes (Al-Qodah et al., 2020; Carlos et al., 2014). Among these processes, the integrated ozone-assisted electrocoagulation technique has shown excellent organic matter removal efficiency for the treatment of textile wastewater (Bilińska et al., 2019), mature landfill leachate (Ghahrchi and Rezaee 2021), steel industry wastewater (Das et al., 2021), greywater (Barzegar et al., 2019) and municipal wastewater (Jin et al., 2020b). Additionally, our previous study has suggested that synergistic reactions between ozone and coagulants (SOC) in the electro-hybrid ozonation-coagulation process (E-HOC) (with Al and stainless steel as anode and cathode, respectively) played a significant role in the removal of organic matter in addition to coagulation, peroxone, molecular ozone oxidation and •OH oxidation from chain reactions during ozonation (Jin et al., 2020b). Although the integrated ozone-assisted electrocoagulation technique showed higher organic matter removal

* Corresponding author: School of Human Settlements and Civil Engineering, Xi'an Jiaotong University, Xi'an, Shaanxi Province 710049, China.
E-mail address: 1721239489@qq.com (P. Jin).

https://doi.org/10.1016/j.watres.2021.117600
Received 19 May 2021; Received in revised form 20 August 2021; Accepted 22 August 2021
Available online 27 August 2021

Abbreviations

BE	EC process with bipolar connection
BE-HOC	E-HOC process with bipolar connection
BQ	p-benzoquinone
CAT	Catalase
DOC	Dissolved organic matter
DMPO	5,5-dimethyl-1-pyrrolidine N-oxide
EC	Electrocoagulation
E-HOC	Electro-hybrid ozonation-coagulation process
EPR	Electron paramagnetic resonance spectroscopy
ESI-MS	Electrospray ionization mass spectrometry
HPLC	High-performance liquid chromatography
IBP	Ibuprofen
ICP-MS	Inductively coupled plasma mass spectrometer
IPA	Isopropanol
ME	EC process with monopolar connection
ME-HOC	E-HOC process with monopolar connection
ROS	Reactive oxygen species
SOC	Synergistic reactions between ozone and coagulants
WWTP	Wastewater treatment plant
XPS	X-ray photoelectron spectroscopy

efficiency, the systems applied in the previous studies were operated in monopolar connection mode (Ghahrchi and Rezaee 2020, 2021; Jin et al., 2020b), which may limit the further improvement of the removal performance.

The electrode arrangement can have a substantial effect on the removal efficiency of the electrochemical processes (Abdessamad et al., 2013; Ghosh et al., 2008). Monopolar electrodes require an external electrical contact to the power supply, and their two faces are active with the same polarity (Kobya et al., 2011). However, in the bipolar arrangement, only the extreme electrodes are connected to the power source (Golder et al., 2007). Every electrode excluding the electrodes at the end acts as an anode on one side and cathode on the other side (Koparal and Öğütveren 2002). Fluoride (Ghosh et al., 2008) and Cr^{3+} (Golder et al., 2007) removal efficiency are higher under bipolar connections than under monopolar connections. However, the monopolar series electrode mode has a higher arsenic removal efficiency compared with bipolar electrodes in serial connections (Kobya et al., 2011). Abdessamad et al. (2013) and Asselin et al. (2008) also indicated that higher organic matter removal performance can be achieved in bipolar electrode systems compared with monopolar electrode systems using either Al or Fe electrodes. Moreover, bipolar arrangements show high energy saving potential (Ghosh et al., 2008) and are easy to maintain in practical applications (Asselin et al., 2008). Nevertheless, there is little comparative information available relating to the removal performance of the E-HOC process with monopolar and bipolar electrodes for the treatment of WWTP effluent. In addition, differences in the hydrolyzed coagulant species generated in different electrode connection configurations also need to be characterized.

In the EC process, electrochemical oxidation of a suitable anode material (Al and Fe) leads to the in situ formation of metal ions serving as coagulants (Heffron et al., 2019). Immediately after the generation of metal ions in the EC process, a series of hydrolyzis reactions occur (Duan and Gregory 2003). Thereafter, many hydrolyzed species including monomers, oligomers and polymeric hydroxyl complexes for both Al and Fe coagulants can be generated from deprotonation and hydroxyl bridging (Duan and Gregory 2003; Yan et al., 2008). However, ozone can react with the hydrolyzed coagulant species to generate

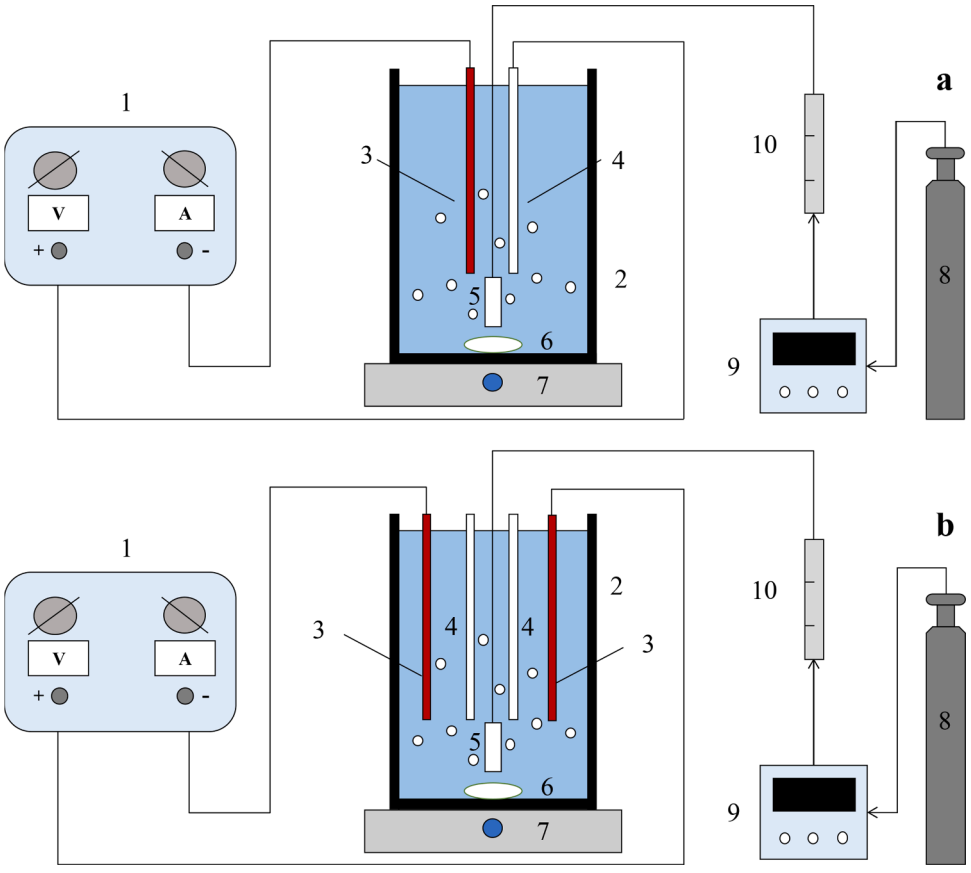

Fig. 1. The bench-scale E-HOC reactor in monopolar (a) and bipolar (b) electrodes connection modes. DC power supply; 2. Reaction unit; 3. Stainless steel electrodes; 4. Iron/Aluminum electrodes; 5. Aerator; 6. Mixer; 7. Magnetic stirring; 8. Oxygen tank; 9. Ozone generator; 10. Glass rotameter.

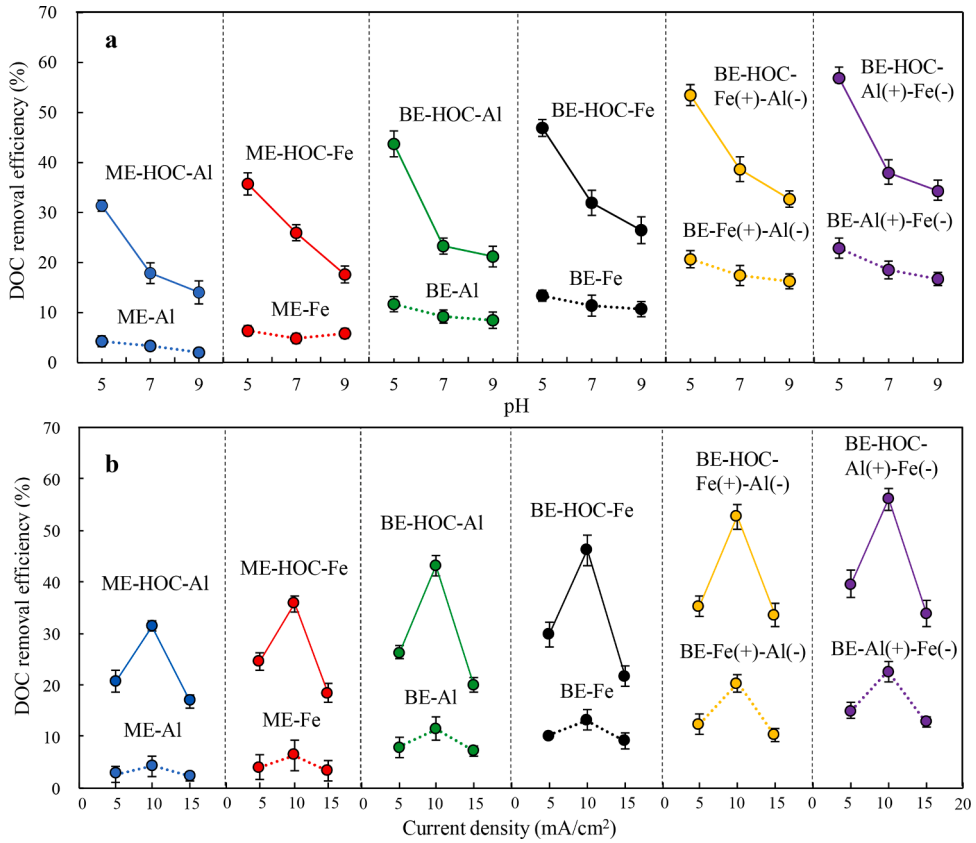

Fig. 2. (a) DOC removal performance for the treatment of WWTP effluent with different processes at different initial pH at a current density of 10 mA/cm^2. (b) DOC removal performance for the treatment of WWTP effluent with different processes at different current densities (5, 10 and 15 mA/cm^2) at initial pH 5.

reactive oxygen species (ROS) in the HOC process (Jin et al., 2020a). The hydrolyzis of metal coagulants in the E-HOC process might be affected by the reactions between the ozone and metal coagulants. Nevertheless, the effect of ozonation on the hydrolyzed species of electro-generated coagulants needs to be further investigated. Furthermore, previous studies have found that the use of Fe and Al as dual-coagulants (i.e., the combined use of different coagulants) is superior for water treatment compared with the use of each coagulant alone (Cheng et al., 2003; Ma et al., 2014). For the E-HOC process, the formation of dual-coagulants can be achieved by simply using two different metal anodes (Fe and Al) at the same time. Generally, characterizing the effects of generated dual-coagulants on the removal efficiency of the E-HOC process is of great practical significance.

The above findings indicated that the E-HOC process can improve the organic matter removal efficiency compared with the EC process. In addition, higher removal efficiency can be obtained in EC with bipolar connection and dual-coagulants mode than that with monopolar connection and single-coagulant mode. There is thus a need to combine the E-HOC process with bipolar connection and dual-coagulants mode to further enhance organic matter removal. In this study, the WWTP effluent organic matter and ibuprofen (IBP) removal efficiency for the E-HOC process with different types of coagulants generated (single-coagulant and dual-coagulants) and different electrode arrangements (monopolar and bipolar connections) was studied. IBP is a common non-steroidal anti-inflammatory drug and an emerging contaminant frequently detected in WWTP effluent and natural waters (Li et al., 2014). The Al and Fe hydrolyzed species were also analyzed using the Ferron assay and electrospray ionization mass spectrometry (ESI-MS) to better characterize the significance of polar types and connection configurations in the E-HOC process. Moreover, the underlying mechanism within the E-HOC process was also elucidated in this study.

2. Materials and methods

2.1. Water samples and experimental setup

WWTP effluent collected from a secondary sedimentation tank in Xi'an, China was used as the raw water. The experiments were carried out in a rectangular batch reactor with dimensions of 10 × 7 × 12 cm (length × width × height) with effective volume of 500 mL (Fig. 1). The experiments were conducted at different initial pH (initial pH = 5, 7 and 9). The detailed information about the raw water quality, experimental setup and operation condition is provided in Text S1.

2.2. Analytical methods

2.2.1. Dissolved organic matter (DOC) and IBP analysis

DOC was measured by a Shimadzu TOC-V_{CPH} analyzer with infrared detection (detection limit 50 μg/L). The DOC analyzer was calibrated with potassium hydrogen phthalate standard solutions before each run. All samples were filtered with a 0.45 μm filter, acidified with H_2SO_4 and purged with nitrogen to remove inorganic carbon before measurement. All analyzes were performed in triplicate for DOC measurements. A high-performance liquid chromatography (HPLC) system was used to measure the concentration of IBP according to Jin et al. (2020b), and detailed information is provided in Text S2.

2.2.2. Al and Fe species detection

Al and Fe species distributions were analyzed through both the Ferron colorimetric method and ESI-MS using a Waters Xevo TQD mass spectrometer. Detailed procedures can be seen in Text S3.

2.2.3. X-ray photoelectron spectroscopy (XPS) and electron paramagnetic resonance spectroscopy (EPR) analysis

An X-ray photoelectron spectrometer was used for the XPS analysis (Thermo Fisher Scientific, UK). Detailed sample preparation and operation procedures are provided in Text S4. A Bruker EMXmicro spectrometer (Germany) was applied for EPR experiments at room temperature. Specific operation parameters are provided in Text S5.

2.2.4. Energy consumption and Faradaic efficiency calculation

The electrical energy per order (E_{EO}) was calculated according to Barazesh et al. (2015), which is defined as the electrical energy (in kWh) required to reduce a contaminant concentration by 1 order of magnitude in 1 m^3 of water. The detailed calculation procedure is provided in Text S6. Faradaic efficiencies (FE) within the reaction systems was calculated according to Ingelsson et al. (2020). Detailed information is provided in Text S7.

3. Results and discussion

3.1. Removal performance of the E-HOC process

The removal performance of the EC and E-HOC processes for the treatment of WWTP effluent at initial pH of 5, 7 and 9 was investigated (Fig. 2a) (pH variation in the different systems at different initial pH was shown in Fig. S1). Fig. 2a shows that both the EC and E-HOC processes exhibited higher DOC removal efficiency at initial pH 5 compared with initial pH 7 and 9. Higher pH can lead to the formation of soluble Al $(OH)_4^-$ or Fe$(OH)_4^-$ ions (Duan and Gregory 2003), which reduced the neutralization capacity of the generated coagulants, thereby decreasing the DOC removal efficiency. Generally, the EC and E-HOC with bipolar connection and dual-coagulant generation model exhibited higher DOC removal efficiency compared with the EC and E-HOC with monopolar connection and single-coagulant generation mode. In addition, E_{EO} was calculated at different initial pH. The results are shown in Table S1. Because of the addition of ozone, higher energy consumption was observed for the E-HOC processes in general (Table S1). For both the EC and E-HOC processes, the bipolar connection exhibited lower energy consumption compared with monopolar connection, which is consistent with the results of Ghosh et al. (2008). In addition, the E-HOC processes with dual-coagulants generation had lower energy consumption compared with the E-HOC with single-coagulant generation.

The removal performance of dissolved organic matter in the WWTP effluent was comparatively investigated for the different processes at different current densities (5, 10 and 15 mA/cm^2) at initial pH 5 (Fig. 2b), which was the optimal initial pH in Fig. 2a. The DOC removal efficiency was higher for the EC processes with 10 mA/cm^2 current density than with current densities of 5 and 15 mA/cm^2. Nevertheless, the highest DOC removal efficiency for the EC processes was less than 25%. The current density is directly related to the efficiency of reactions occurring on the anode surface (Lacasa et al., 2012), and Faradaic efficiency (FE) of different processes with different current densities at initial pH 5 was calculated (Table S2). Table S2 showed that lower FE can be obtained with the increase of current density in general, which indicated increased passivation effects on the surface of electrodes. At a current density of 15 mA/cm^2, the passivation of the electrodes became serious, which resulted in lower DOC removal efficiency at 15 mA/cm^2. This was consistent with the results of Chen et al. (2020) and Dubrawski et al. (2015). The processes with Fe as anode exhibited lower FE according to Table S2. Ingelsson et al. (2020) reported that low efficiencies are more frequently observed in Fe-EC than in Al-EC. Previous studies indicated that once a surface layer has formed, electrochemically produced Fe(II) was trapped within the lattice of the surface layer, which hindered the dissolved Fe from diffusing to the bulk solution accelerating the surface layer buildup (Bandaru et al., 2020; Müller et al., 2019). In addition, the lower removal efficiency at a current density of 15 mA/cm^2 may also be attributed to the water oxidation at the anode, which inhibits the production of Al^{3+} and Fe^{3+} (Mouedhen et al., 2008). Previous studies also implied that higher current density can resulted in the charge reversal in the EC process at initial pH 5 (Harif et al., 2012; Jin et al., 2020b), which may also lead to the poor DOC removal at higher current density.

The removal efficiency was higher for the EC processes with bipolar connection than with monopolar connection at different current densities, and the concentrations of Al_T and Fe_T in the treated water were similar for the EC processes with bipolar and monopolar connection at the same current density (Table S3). These results were consistent with those of Hu et al. (2016) showing that a larger solution-electrode interface can be provided for electrochemical reactions in the bipolar EC process. Hu et al. (2016) also suggested that Al^{3+} and OH^- can be generated from the bipolar electrode surface more homogeneously and can be fully arranged in bulk solution, which is more favorable for Al_{13} formation to enhance coagulation. Furthermore, the bipolar EC processes had higher DOC removal efficiency with dual-coagulant generation than with single-coagulant generation. Ma et al. (2014) suggested that the positively charged hydrolyzates of Fe can accelerate the cross-linking and clustering of organic-Al complexes and Al hydrolyzates. In the case of EC with dual coagulants generation of the BE-Al (+)-Fe(-) process, the Al and Fe electrodes were placed close to the stainless steel anode and cathode, respectively. Similarly, in the BE-Fe (+)-Al(-) process, the Fe and Al electrodes were placed close to the stainless steel anode and cathode, respectively.

According to Fig. 2b, it can be seen that significantly higher DOC removal efficiency was observed for the E-HOC processes than for the EC processes at the same current densities. Furthermore, as the current densities increased, the DOC removal efficiency improved and peaked at 31.38%, 35.69%, 43.67%, 46.86%, 53.44% and 56.89% at 10 mA/cm^2 in the ME-HOC-Al, ME-HOC-Fe, BE-HOC-Al, BE-HOC-Fe, BE-HOC-Al (+)-Fe(-) and BE-HOC-Fe(+)-Al(-) processes, respectively. Compared with the E-HOC process with monopolar electrodes (ME-HOC), the E-HOC process with bipolar electrodes also exhibited higher removal efficiency at different densities (Fig. 2b), and the concentrations of Al_T and Fe_T in treated water were similar for the ME-HOC and BE-HOC processes at the same current density (Table S4). With Al electrodes, the average DOC removal efficiency was 6.03%, 12.29% and 3.39% higher for the BE-HOC process than for the ME-HOC process with current densities of 5, 10 and 15 mA/cm^2, respectively. Moreover, the results were similar when Fe electrodes were used. Specifically, the average DOC removal efficiency was 5.70%, 11.17% and 3.70% higher for the BE-HOC process than for the ME-HOC process with current densities of 5, 10 and 15 mA/cm^2, respectively. In addition, FE was higher with bipolar connection than corresponding monopolar configuration in general (Table S2), which was consistent with Asselin et al. (2008).

Although lower FE was obtained for ME-HOC and BE-HOC with Fe electrodes (Table S2), the ME-HOC and BE-HOC processes achieved higher DOC removal efficiency with Fe electrodes than with Al electrodes. This can be ascribed to the higher hydrolyzis rate of generated Fe species than that of generated Al species (Wang et al., 2013). In addition, generated Fe species possess a higher content of surface hydroxyl groups that can react with ozone compared with generated Al species (Jin et al., 2020a; Wang et al., 2013). According to Fig. 2b, it is the same with the EC processes that the generation of dual-coagulants in the bipolar connection mode, which are released from both the electrolysis of the Al and Fe electrodes, can greatly improve the average DOC removal efficiency under different densities in the BE-HOC process.

3.2. Hydrolyzed species analysis

The generated hydrolyzed coagulant species can affect the removal performance of the EC processes (Hu et al., 2016), and there are interactions between ozone and hydrolyzed coagulant species within the E-HOC process (Jin et al., 2020b). To get more insight into the E-HOC process, the Al/Fe species distributions were obtained through the

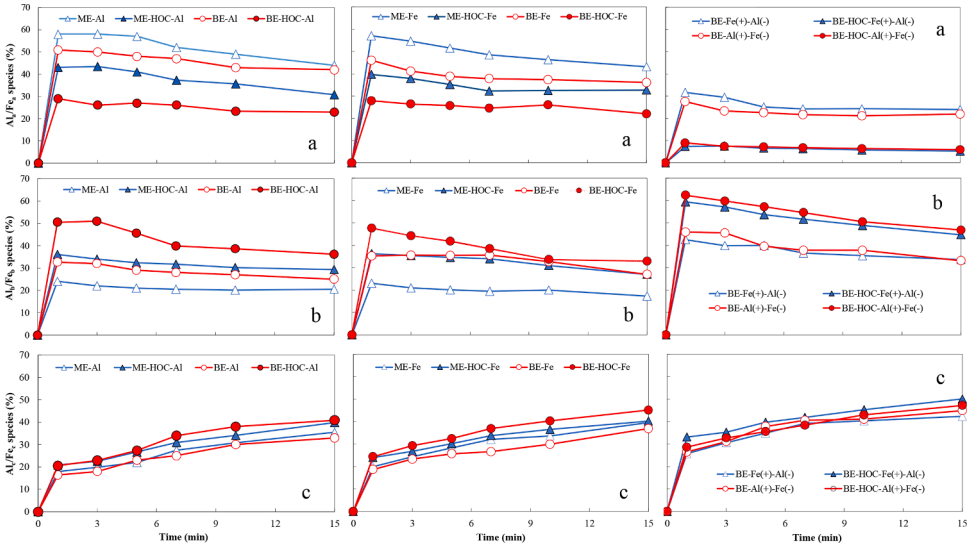

Fig. 3. Characterization of Al/Fe speciation through the Ferron assay. (a) Al_a/Fe_a, (b) Al_b/Fe_b, (c) Al_c/Fe_c. Reaction conditions: initial pH = 5, ozone dosage 11.52 mg/L, reaction duration 15 min, current density 10 mA/cm^2.

Al/Fe-Ferron method quantitatively in ultrapure water system without the interference of organic matter at initial pH 5 (Fig. 3). The distributions of Al/Fe species at 1 min at different initial pH are shown in Fig. S2. As shown in Fig. 3, as the reaction time increased, the dominant Al/Fe species transformed from monomer (Al_a/Fe_a) to medium polymers (Al_b/Fe_b) and subsequently to larger polymers or Al(OH)$_{(s)}$ (Al_c/Fe_c). Initially, the monomer and medium polymer increased rapidly and reached a maximum at 1 min in all of the EC and E-HOC processes at initial pH 5 and decreased as the reaction time increased. The distributions of monomer and medium polymer were similar. Larger polymer increased throughout all the EC and E-HOC processes. Fig. 3 also revealed that the addition of ozone promoted Al/Fe polymer formation in all of the E-HOC processes. Furthermore, compared with monopolar connection, the generation of Al_b/Fe_b was increased in the EC and E-HOC processes with bipolar electrodes (Fig. 3). These results were consistent with those of Hu et al. (2016) showing that yields of Al_b species were higher for EC with bipolar connection than EC with monopolar connection. Additionally, the formation of Al_b/Fe_b can also be enhanced in the dual-coagulant generation mode according to Fig. 3.

The content of Al_b has been reported to be correlated to the tridecamer ($Al_{13}O_4(OH)_{24}^{7+}$, often denoted as Al_{13}) (Duan and Gregory 2003; Yan et al., 2008). Al_{13} is considered a highly efficient polymeric aluminum species for coagulation not only because of its strong charge neutralization capacity (Lin et al., 2008) but also its nucleation ability to form flocs with soluble organic matter to produce colloids and precipitates efficiently (Yan et al., 2008). Because of the advantages of Al_{13} polycation in coagulation, preformed Al_{13} species have been applied as coagulants to enhance the removal performance of coagulation (Jin et al., 2020b; Xu et al., 2011). Our previous study also found that preformed Al_{13} exhibited higher catalytic ability for ozonation compared with in situ generated Al species from $AlCl_3 \bullet 6H_2O$ (Jin et al., 2019). In this case, the EC and E-HOC with bipolar connections and the dual-coagulant generation mode produced more Al_b/Fe_b. Therefore, higher organic matter removal efficiency can be achieved according to Fig. 2. The generated Al/Fe species of different processes at initial pH 7 and pH 9 through the Ferron assay were also compared. The results can be seen in Fig. S3 and Fig. S4. In general, higher Al_b/Fe_b can also be obtained from bipolar connection and dual-coagulant generation mode at initial pH 7 and 9. In addition, the addition of ozone can also lead to the increased formation of Al/Fe polymer in all the E-HOC processes. Compared with Al_b/Fe_b generation at initial pH 7 and 9, higher Al_b/Fe_b can be formed at initial pH 5, which can lead to higher DOC removal efficiency for the EC and E-HOC process at initial pH 5.

Table 1
Distribution of hydrolyzed Al species in the different processes at different initial pH (current density 10 mA/cm^2, ozone dosage 11.52 mg/L).

	Process	Al_{3-5}	Al_{6-10}	Al_{11-21}	Al_u
pH 5	ME-Al	1.79%	77.21%	9.24%	11.76%
	BE-Al	15.47%	36.71%	18.19%	29.63%
	ME-HOC-Al	17.18%	14.04%	23.76%	45.02%
	BE-HOC-Al	18.89%	10.79%	25.36%	44.96%
pH 7	ME-Al	1.80%	44.38%	19.70%	34.12%
	BE-Al	4.84%	29.76%	26.59%	38.81%
	ME-HOC-Al	11.30%	9.85%	32.27%	46.59%
	BE-HOC-Al	–	7.88%	40.79%	51.33%
pH 9	ME-Al	8.61%	17.52%	20.18%	53.69%
	BE-Al	6.02%	13.67%	22.39%	57.92%
	ME-HOC-Al	4.51%	10.56%	26.76%	58.17%
	BE-HOC-Al	5.11%	4.18%	29.54%	61.17%

Table 2
Distribution of hydrolyzed Fe species in the different processes at different initial pH (current density 10 mA/cm^2, ozone dosage 11.52 mg/L).

	Process	Fe_1	Fe_2	Fe_3	Fe_4	Fe_u
pH 5	ME-Fe	3.79%	38.53%	17.73%	5.40%	34.54%
	BE-Fe	6.10%	11.97%	41.69%	3.49%	36.75%
	ME-HOC-Fe	3.53%	8.82%	39.88%	3.98%	43.79%
	BE-HOC-Fe	4.84%	40.23%	–	10.46%	44.47%
pH 7	ME-Fe	8.83%	10.82%	29.49%	5.57%	45.29%
	BE-Fe	19.15%	12.73%	4.73%	6.09%	57.29%
	ME-HOC-Fe	4.90%	14.98%	9.73%	6.85%	63.54%
	BE-HOC-Fe	3.21%	14.17%	9.71%	8.12%	64.79%
pH 9	ME-Fe	–	30.26%	6.37%	3.85%	59.52%
	BE-Fe	5.52%	10.04%	18.43%	4.92%	61.09%
	ME-HOC-Fe	7.08%	12.77%	10.79%	5.06%	64.30%
	BE-HOC-Fe	5.29%	12.85%	4.79%	9.74%	67.32%

The effect of ozonation on electro-generated Al and Fe hydrolyzis was further investigated by ESI-MS. Fig. S5~S16 show the ESI-MS spectra of Al and Fe speciation. According to the ESI-MS spectra (Fig. S5~S10), the Al species were classified into four categories: small polymeric aluminum species (Al_3-Al_5), median polymeric aluminum species (Al_6-Al_{10}), large polymeric aluminum species (Al_{11}-Al_{21}) and undetected part (Al_u: $Al(OH)_3$ and $Al(OH)_4^-$) (Zhao et al., 2009a). Based on the ESI-MS spectra (Fig. S11~S16), Fe species can be divided into

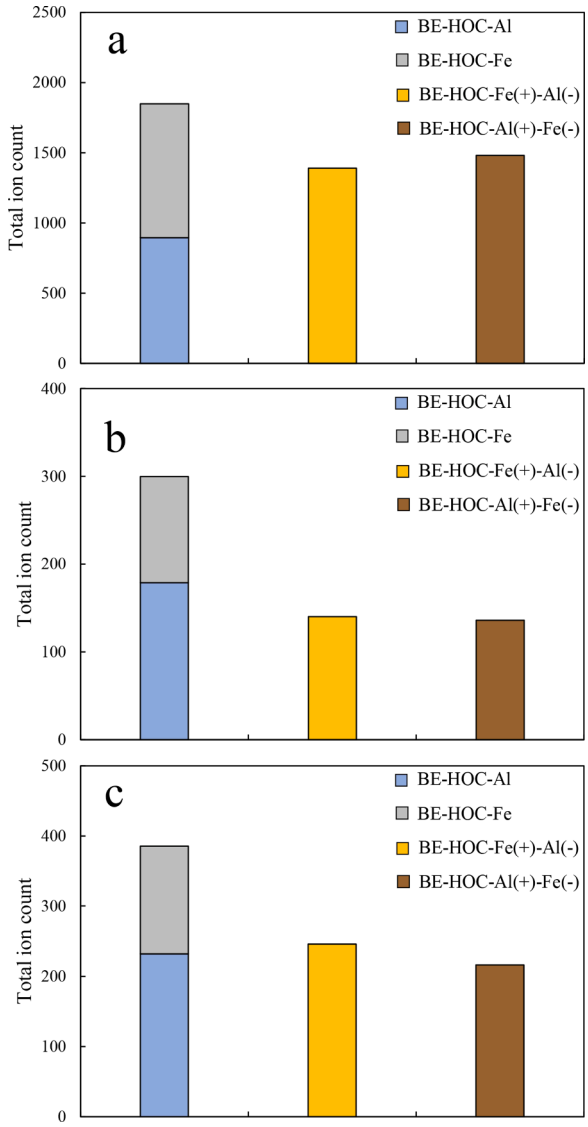

Fig. 4. Total ion count (TIC) in the spectra of the BE-HOC-Al, BE-HOC-Fe, BE-HOC-Fe(+)-Al(-) and BE-HOC-Al(+)-Fe(-) processes. (a) initial pH 5, (b) initial pH 7, (c) initial pH 9. Spectra were recorded in positive ion mode. All samples were filtrated before ESI-MS analysis. The samples for ESI-MS analysis were taken at one minute during the reactions. Reaction conditions: ozone dosage 11.52 mg/L, current density 10 mA/cm^2.

monomeric Fe species (Fe_1), dimeric Fe species (Fe_2), trimeric Fe species (Fe_3), tetrameric Fe species (Fe_4) and undetected part (Fe_u: $Fe(OH)_3$ and $Fe(OH)_4^-$) (Hellman et al., 2006; Ma et al., 2014). The distributions of Al and Fe species in the EC and E-HOC processes at different initial pH are provided in Table 1 and Table 2, respectively.

As shown in Table 1, in both the EC-Al and E-HOC-Al processes, the polymer Al (Al_{11}-Al_{21}) and the undetected part (Al_u) were greater with bipolar connection at different initial pH. This may stem from the higher pH within the bipolar connection process for the same initial pH (Fig. S1), which accelerates the hydrolyzis polymerization reaction. Ghosh et al. (2008) also confirmed that the pH of the solution was higher for bipolar connection than for monopolar connection. In the E-HOC-Al process, Al^{3+} produced by the electrolytic dissolution of the anode immediately undergoes spontaneous hydrolyzis reactions that form various monomeric species and subsequently aggregate into multiple polymeric species, such as small and median polymeric Al (Mouedhen et al., 2008). Al is usually present in the form of Al^{3+}, and six water molecules are combined to produce $Al(OH)_6$ octahedra in aqueous solution (Tang et al., 2015). As the pH increases, the six water molecules around Al^{3+} can gradually deprotonate and form a series of Al-OH compounds. Al-OH compounds can then form a pair of octaeth structures by forming OH bridges (Baes and Mesmer, 1976). Therefore, hydrolyzis and polymerization processes were accelerated in the bipolar connection process because of the higher pH compared with monopolar connection.

ESI-MS was also applied to compare the hydrolyzis behaviors of electro-generated Al and Fe in the BE-HOC-Al, BE-HOC-Fe, BE-HOC-Fe(+)-Al(-) and BE-HOC-Al(+)-Fe(-) processes to provide further insight into the hydrolyzis of Fe and Al as dual-coagulants (Fig. S17, Fig. S18 and Fig. S19). The total ion count (TIC) in the spectra of the BE-HOC-Al, BE-HOC-Fe, BE-HOC-Fe(+)-Al(-) and BE-HOC-Al(+)-Fe(-) processes at different initial pH is shown in Fig. 4. At the same initial pH, the TIC value of Al and Fe in all the BE-HOC-Fe(+)-Al(-) or BE-HOC-Al(+)-Fe(-) process was less than the sum of the TIC values of the BE-HOC-Al and BE-HOC-Fe processes (Fig. 4). This finding was consistent with the result of Ma et al. (2014), which indicates that the coexistence of Al and Fe hydrolyzis can improve the precipitation of coagulants compared with Fe or Al alone. Thus, dual-coagulant generation confers a superior coagulation ability and provides a practical approach for controlling coagulant residues.

According to Table 1, comparison of the EC-Al and E-HOC-Al processes also revealed that the addition of ozone leads to a reduction in the proportion of medium polymer (Al_6-Al_{10}), whereas the proportion of large polymer (Al_{11}-Al_{21}) and the undetected part (Al_u) increase at different initial pH in general. This indicates that the addition of ozone is beneficial to the formation of higher polymerized Al species (Al_{11}-Al_{21} and Al_u). The same pattern was also observed in the EC-Fe and E-HOC-Fe processes. According to Table 2, the addition of ozone and bipolar connection led to increases in the higher polymeric Fe species and the undetected part. This also further suggested that ozonation and bipolar connection are beneficial to the formation of higher polymerized Fe species. It was proved that hydrolyzed Al species and Fe species can activate ozone to generate ROS (Jin et al., 2020a). Thus, the hydrolyzed metal coagulant species might change during the reactions between ozone and hydrolyzed coagulant species. As a result, the increased generation of polymerized hydrolyzed species with the addition of ozone, such as Al_b/Fe_b, can further enhance the coagulation efficiency of the E-HOC process.

3.3. ROS generation in the E-HOC process

The degradation of IBP during the ME-HOC-Al, BE-HOC-Al, ME-HOC-Fe, BE-HOC-Fe, BE-HOC-Fe(+)-Al(-) and BE-HOC-Al(+)-Fe(-) processes is compared in Fig. 5 to characterize differences between the various E-HOC processes at initial pH 5, which is the optimal initial pH for the E-HOC process according to Fig. 2. IBP is one of the pharmaceutical compounds, which exhibited low reactivity with ozone ($k_{O3,\ IBP}$ = 9.1 $M^{-1}s^{-1}$) but high reactivity with •OH ($k_{•OH,\ IBP}$ = 7.4 × 10^9 $M^{-1}s^{-1}$) (Li et al., 2014). In addition, chemical coagulation and EC can hardly remove IBP (Jin et al., 2020a), Therefore, IBP was used as a model compound for the detection of ROS. In addition, as presented in Fig. 5, IBP removal followed pseudo-first-order kinetics for all the E-HOC processes. The degradation rates of different processes are summarized in Table 3. It can be observed that the degradation rate of IBP was significantly enhanced in the BE-HOC-Fe(+)-Al(-) and BE-HOC-Al(+)-Fe(-) processes (k_{obs} = 0.3666 min^{-1} and 0.3737 min^{-1}, respectively) compared with the ME-HOC-Al, ME-HOC-Fe, BE-HOC-Al and BE-HOC-Fe processes (k_{obs} = 0.2281 min^{-1}, 0.2661 min^{-1}, 0.3094 min^{-1} and 0.3209 min^{-1}, respectively). These results were consistent with the DOC removal performance for the WWTP effluent using these E-HOC processes (Fig. 2).

To further verify the generation of ROS, trapping experiments were conducted at initial pH 5 by adding excess isopropanol (IPA), catalase (CAT) and p-benzoquinone (BQ) (as •OH, H_2O_2 and $•O_2^-$ scavengers,

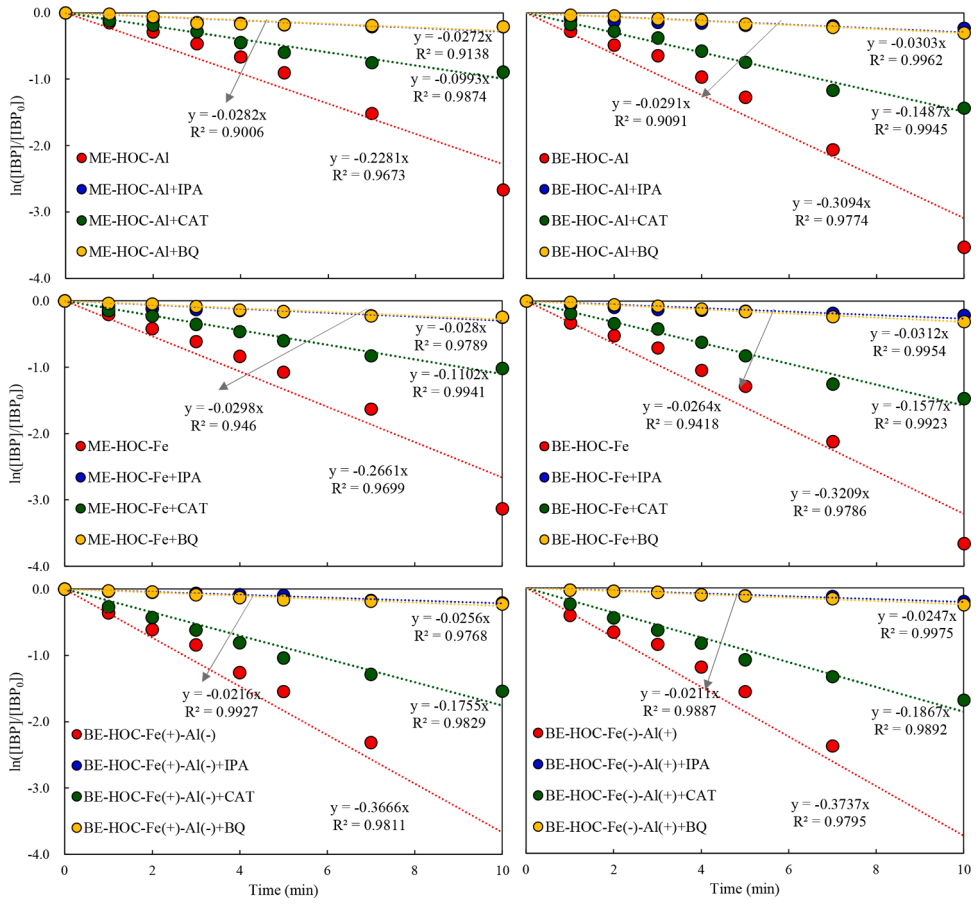

Fig. 5. Pseudo-first-order rate constant (k_{obs}) analysis in the different E-HOC processes. Reaction conditions: current density 10 mA/cm^2, initial pH = 5, ozone dosage 11.52 mg/L, [IBP] = 50 μM, [IPA] = 5 mM, [CAT] = 300 U/mL, [BQ] = 10 mM, reaction duration 10 min.

Table 3
Pseudo-first-order rate constant of the different E-HOC processes for the degradation of IBP. (initial pH 5, current density 10 mA/cm^2, ozone dosage 11.52 mg/L, [IBP] = 50 μM, [IPA] = 5 mM, [CAT] = 300 U/mL, [BQ] = 10 mM, reaction duration 10 min).

Scavengers	Scavenged species	k_{obs} (min^{-1})					
		ME-HOC-Al	ME-HOC-Fe	BE-HOC-Al	BE-HOC-Fe	BE-HOC-Fe(+)-Al(-)	BE-HOC-Fe(-)-Al(+)
–	/	0.2281	0.2661	0.3094	0.3209	0.3666	0.3737
IPA	•OH	0.0282	0.0298	0.0291	0.0264	0.0216	0.0211
CAT	H_2O_2	0.0993	0.1102	0.1487	0.1577	0.1755	0.1867
BQ	$•O_2^-$	0.0272	0.028	0.0303	0.0312	0.0256	0.0247

respectively) before starting the E-HOC experiments Jin et al., 2020a; Xiong et al., 2018). The results are shown in Fig. S20. The degradation of IBP was inhibited in the presence of IPA, CAT and BQ, indicating that •OH, H_2O_2 and $•O_2^-$were generated in all of the E-HOC processes. The degradation of IBP was largely inhibited by IPA and BQ, indicating that •OH and $•O_2^-$ played a key role in the degradation of IBP. Typically, $•O_2^-$ can transform into •OH in aqueous solution (Eqs. (1)-((2)) (Li et al., 2018). To quantitatively analyze the contribution of •OH, the proportion of •OH oxidation was calculated by •OH quenching experiments (E-HOC+IPA), and •OH oxidation accounted for 87.64%, 88.80%, 90.59%, 91.77%, 94.11% and 94.35% contribution for the ME-HOC-Al, BE-HOC-Al, ME-HOC-Fe, BE-HOC-Fe, BE-HOC-Fe(+)-Al(-) and BE-HOC-Al(+)-Fe(-) processes, respectively, which further indicated that IBP was mainly eliminated by •OH oxidation. It can be seen that the BE-HOC processes can significantly improve the formation of •OH compared with the ME-HOC processes. The amount of •OH formed was also greater when dual-coagulants were generated relative to when only Fe or Al coagulant was generated.

$$•O_2^- + H^+ \rightarrow H_2O_2 + O_2 \quad (1)$$

$$H_2O_2 + •O_2^- + H^+ \rightarrow •OH + O_2 + H_2O \quad (2)$$

EPR experiments were performed using 5,5-dimethyl-1-pyrrolidine N-oxide (DMPO) as a spin-trapping agent in these E-HOC processes to provide direct evidence for ROS generation. Three different signals representing DMPO-•OH adducts (marked with the circle symbol), carbon-centered radical adducts (marked with arrow symbol) and oxidized DMPO radicals (marked with rectangle symbol) are shown in Fig. 6. The oxidation of DMPO was featured by a three-line spectrum (Feng et al., 2016; Xiong et al., 2018). In addition, the attack of carbon-containing compounds by •OH results in the appearance of carbon-centered radical adducts with a six-peak spectrum (Dong et al., 2014). Besides, strong signals of the DMPO-•OH adduct with a peak intensity ratio of 1:2:2:1 were also detected (Tan et al., 2018).

In Fig. 6, the signal of DMPO-•OH and DMPO-•CH_3 indicated the presence of •OH in all of the E-HOC processes, which was consistent with the results of the quenching experiments. Fig. 6 shows that the signal intensities of DMPO-•OH adduct were noticeably stronger in the

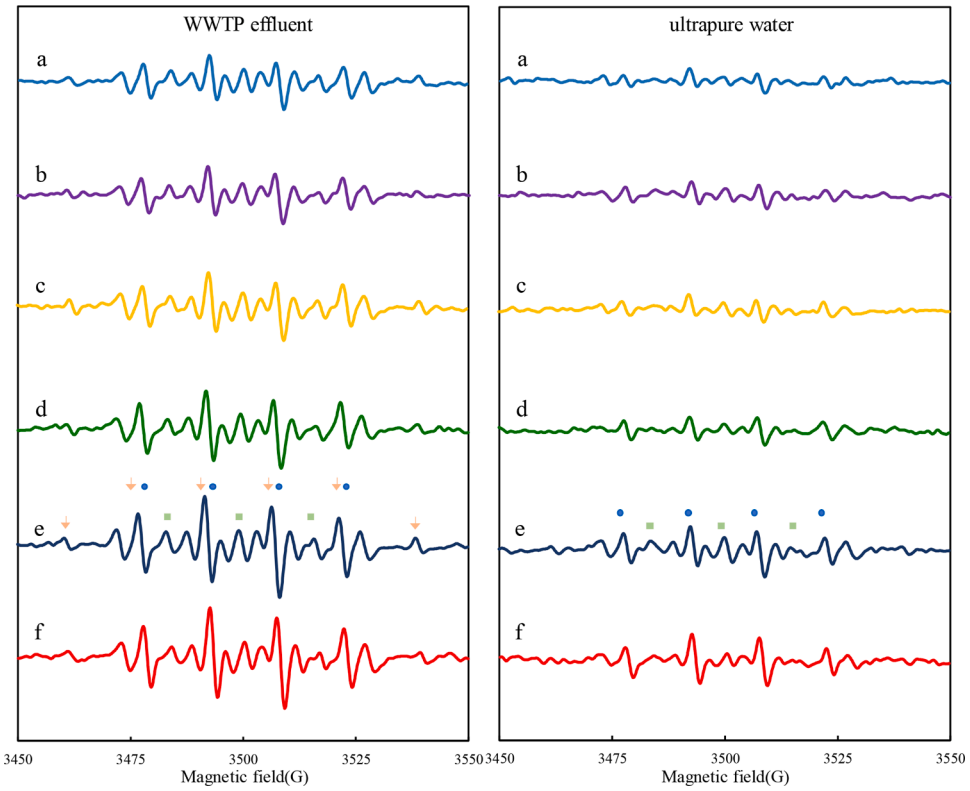

Fig. 6. EPR spectra detected in the E-HOC process. (a) ME-HOC-Al, (b) ME-HOC-Fe, (c) BE-HOC-Al, (d) BE-HOC-Fe, (e) BE-HOC-Fe (+)-Al(-), (f) BE-HOC-Al(+)-Fe(-). DMPO-•OH adducts (marked with the circle symbol), carbon-centered radical adducts (marked with arrow symbol) and oxidized DMPO radicals (marked with rectangle symbol). Reaction conditions: current density 10 mA/cm^2, ozone dosage 11.52 mg/L, initial pH = 5. Samples for EPR test were taken at the 5th min during the reactions.

BE-HOC-Fe(+)-Al(-) and BE-HOC-Al(+)-Fe(-) processes than in the ME-HOC and BE-HOC processes in both WWTP effluent and the ultrapure water system. This result further confirmed that dual-coagulant generation was more efficient for decomposing ozone to generate •OH compared with single Fe or Al coagulant generation. Bing et al. (2015) reported that the synergism of aluminum and iron onto Fe_2O_3/A-l_2O_3@SBA-15 enhanced the formation of ROS compared with Fe_2O_3@SBA-15, Al_2O_3@SBA-15 and SBA-15, and led to the highest reactivity, indicating that the combination of both Lewis sites of iron and aluminum improved the generation of ROS. Ozone has also been reported to act as a Lewis base that can replace the surface hydroxyls, decompose on Lewis acid sites, and convert into •OH_{ads} and O_2•$^-$ on Fe_2O_3 as well as surface atomic oxygen species on Al_2O_3 (Bing et al., 2015).

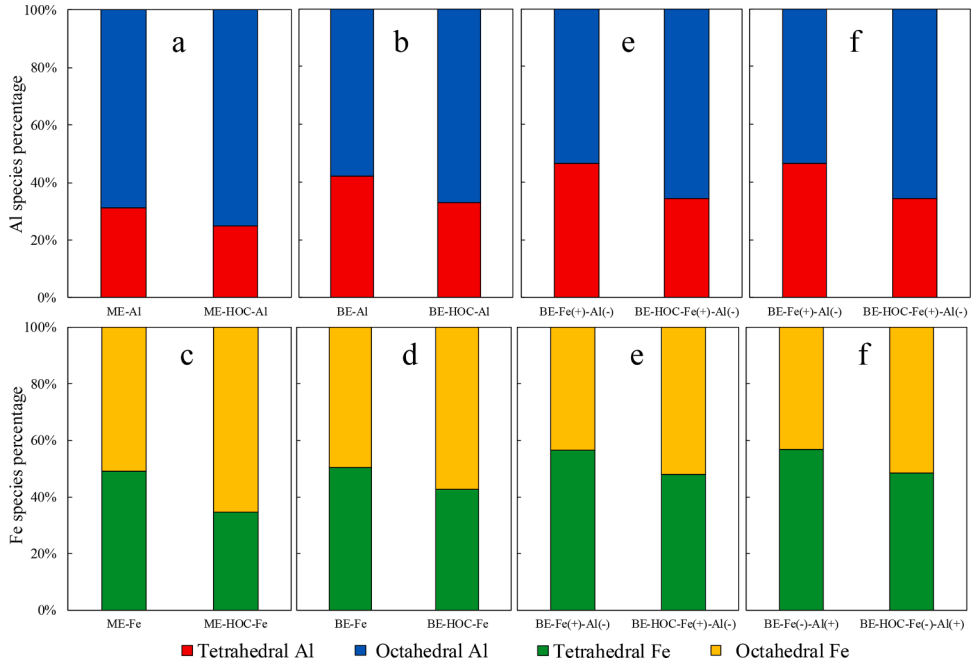

Fig. 7. Proportions of Al and Fe species in the different E-HOC processes. (a) MEAl vs. ME-HOC-Al, (b) BE-Al vs. BE-HOC-Al, (c) ME-Fe vs. ME-HOC-Fe, (d) BE-Fe vs. BE-HOC-Fe, (e) BE-Fe(+)-Al(-) vs. BE-HOC-Fe(+)-Al(-) and (f) BEAl(+)- Fe(-) vs. BE-HOC-Al(+)-Fe(-). Reaction conditions: initial pH = 5, ozone dosage 11.52 mg/L, reaction duration 10 min, current density 10 mA/cm^2.

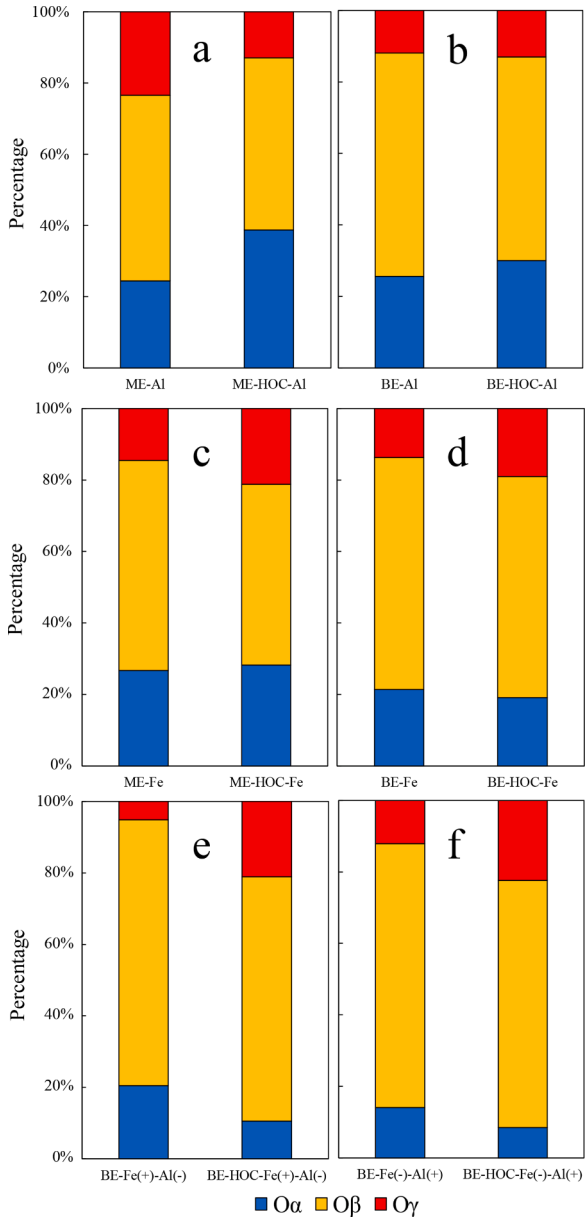

Fig. 8. Proportions of different O species in the different E-HOC processes. (a) MEAl vs. ME-HOC-Al, (b) ME-Fe vs. ME-HOC-Fe, (c) BE-Al vs. BE-HOC-Al, (d) BE-Fe vs. BE-HOC-Fe, (e) BE-Fe(+)-Al(-) vs. BE-HOC-Fe(+)-Al(-) and (f) BEAl (+)- Fe(-) vs. BE-HOC-Al(+)-Fe(-). Reaction conditions: initial pH = 5, ozone dosage 11.52 mg/L, reaction duration 10 min, current density 10 mA/cm^2.

According to Fig. 6, the signal intensities of the BE-HOC processes were greater than those of the ME-HOC processes for DMPO-•OH adduct, indicating that more •OH was generated in the BE-HOC processes. The greater surface area associated with bipolar connection compared with monopolar connection is conducive to anodic oxidation, which contributed to the increase in the current flow in solution and the electrochemical dissolution rate on the anode (Mavré et al. 2010). Meanwhile, the electrode corrosion is greater for bipolar connection than for monopolar connection under the same current density (Ghosh et al., 2008). In addition, it was also observed that the pH of the solution was higher for bipolar connection than for monopolar connection (Fig. S1). The higher OH^- concentration obtained with the higher pH facilitated the initiation of the chain reactions for generating •OH (Chen et al., 2016). According to Fig. 6, the signals of •OH in the WWTP effluent system were clearly stronger than those in the ultrapure water system, which can be attributed to the overlapping of the DMPO-•CH_3 and DMPO-•OH adducts. Based on Fig. 3, Table 1 and Table 2, greater numbers of polymerized hydrolyzed Al/Fe species can be generated with bipolar connection and in the dual-coagulant generation mode. Fig. 6 further proved that higher catalytic ability for ozonation in the HOC process can be achieved with enhanced polymerized hydrolyzed species generation.

3.4. Proposed mechanism within the E-HOC process

To elucidate the mechanism within the E-HOC process, the proportions of hydrolyzed Al/Fe species in the ME-HOC-Al, BE-HOC-Al, ME-HOC-Fe, BE-HOC-Fe, BE-HOC-Fe(+)-Al(-) and BE-HOC-Al(+)-Fe(-) processes were verified to reveal the active reaction sites between hydrolyzed Al/Fe species and ozone, and quantitative analysis was carried out by XPS (Fig. S21, Fig. S22). As shown in Fig. S21, two overlapping bands associated with two different Al 2p transitions with binding energies of 73.1 eV and 74.2 eV were observed, which represented Al^{IV} and Al^{VI}, respectively (Duong et al., 2005; Lin et al., 2014). As can be seen in Fig. S22, the Fe 2p XPS spectra were separated into two types of peaks after fitting, which can be assigned to Fe 2p3/2 (710–720 eV) and Fe 2p1/2 (720–735 eV), respectively (Leveneur et al., 2011). The characteristic XPS spectra peaks for the different processes varied little. The ratio of hydrolyzed Al and Fe species can be obtained after Gaussian fitting using XPS peak software (Fig. 7).

As shown in Fig. 7, the ratios of tetrahedral Al decreased in the ME-HOC-Al, BE-HOC-Al, BE-HOC-Fe(+)-Al(-) and BE-HOC-Al(+)-Fe(-) processes compared with the relative EC processes by 6.25%, 9.14%, 12.14% and 10.33%, respectively. In addition, the ratios of tetrahedral Fe were also reduced in the ME-HOC- Fe, BE-HOC- Fe, BE-HOC-Fe(+)-Al (-) and BE-HOC-Al(+)-Fe(-) processes compared with the relative EC processes by 14.33%, 7.77%, 8.63% and 8.45%, respectively. The results indicated that tetrahedral Al/Fe may be the key species reacting with O_3. Compared with octahedral sites, previous studies have shown that surface tetrahedral sites are stronger Lewis acid sites, which are believed to be significant active sites in catalytic ozonation compared with surface Al in octahedral sites (Bing et al., 2017; Sohlberg et al., 1999). Therefore, the presence of O_3 can improve the reaction with tetrahedral Al/Fe and accelerate the generation of •OH. It can be observed that dual-coagulant generation in the EC or E-HOC process had more tetrahedral Al/Fe, which resulted in higher catalytic reactivity and enhanced •OH formation compared with single-coagulant generation. Meanwhile, the ratio of tetrahedral Al/Fe was greater in the bipolar pattern than in the monopolar pattern, which indicated that the bipolar connection could also enhance catalytic performance.

Additionally, the O1s spectra of the ME-HOC-Al, BE-HOC-Al, ME-HOC-Fe, BE-HOC-Fe, BE-HOC-Fe(+)-Al(-) and BE-HOC-Al(+)-Fe(-) processes are shown in Fig. 8. Based on Fig. S23, the O1 s spectra show three fitted peaks at 530.7 eV (lattice oxygen (O_α)), 531.5 eV (surface hydroxyl group (O_β)) and 532.4 eV (adsorbed water (O_γ)) (Ding et al., 2016). It can be found the addition of O_3 reduced the ratio of surface hydroxyl groups (O_β) on hydrolyzed coagulants, which was attributed to the reactions between O_3 and surface hydroxyl groups. Therefore, it can be implied the surface hydroxyl groups were the main active sites reacting with O_3 for the generation of •OH, which is consistent with the results obtained by Zhao et al. (2015). Compared with single-coagulant generation, dual-coagulant generation had a higher surface hydroxyl group ratio, which resulted in greater ROS formation.

Based on the results described above, the reaction mechanism of the E-HOC process was proposed Fig. 9). In the E-HOC process, Al^{3+} and/or Fe^{3+} can be electro-generated. Thereafter, hydrolyzis of the generated metal ions occurred automatically through hydration to form hydroxyl groups (Duan and Gregory 2003). Fig. 7 and Fig. 8 indicated that the reactions between hydrolyzed species and ozone within the E-HOC process occurred on the surface hydroxyl groups. Because of the acidic condition of the aqueous solution (pH = 5 in this case), the primary

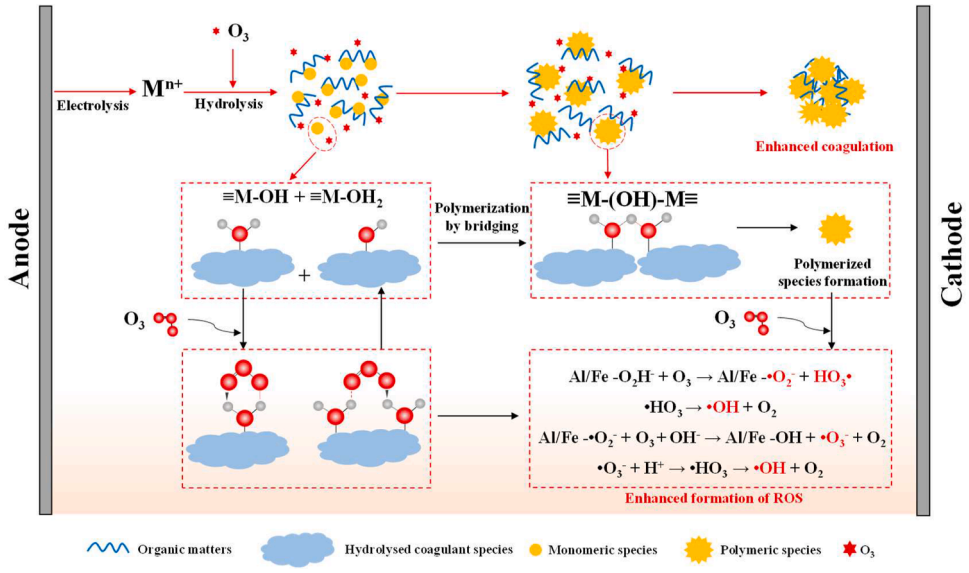

Fig. 9. Proposed mechanism within the E-HOC processes.

surface groups of the hydrolyzed species are the surface protonated hydroxyl groups. Zhao et al. (2009b) suggested that ozone can interact with the surface protonated hydroxyl groups on the catalysts driven by electrostatic force and/or hydrogen bonding. This interaction resulted in the enhanced formation of $•O_3H$, $•O_3^-$ and •OH (Eq. (3)-((6)) Jin et al., 2020a), which improved the oxidation ability of the E-HOC system. Furthermore, the formation of surface -OH groups can also be enhanced during the generation of ROS (Eq. (3)-((5)). Subsequently, bonds between hydrolyzed metal species can be formed between -OH and protonated -OH (-OH_2), leading to the formation of -O_3H_2- bridges that can release H_2O to generate OH bridges (Eq. (7)) (Yu et al., 2016). As a result, the presence of O_3 can promote the formation of polymerized Al/Fe species, and the coagulation performance can be also improved for the E-HOC process. The E-HOC process in bipolar and/or dual-coagulant generation mode further enhanced the formation of polymerized Al/Fe species, and thus improved the coagulation and catalytic ability within the E-HOC process (Fig. 9).

$$\text{Al/Fe -}O_2H^- + O_3 \rightarrow \text{Al/Fe -}•O_2^- + HO_3• \quad (3)$$

$$•HO_3 \rightarrow •OH + O_2 \quad (4)$$

$$\text{Al/Fe -}•O_2^- + O_3 + OH^- \rightarrow \text{Al/Fe -OH} + •O_3^- + O_2 \quad (5)$$

$$•O_3^- + H^+ \rightarrow •HO_3 \rightarrow •OH + O_2 \quad (6)$$

$$\equiv\text{M-OH} + \equiv\text{M-}OH_2 \rightarrow \equiv\text{M-}(O_3H_2)\text{-M}\equiv \rightarrow \equiv\text{M-(OH)-M}\equiv + H_2O \quad (7)$$

4. Conclusions

The E-HOC processes exhibited significantly higher WWTP effluent and IBP removal efficiency compared with EC processes at different current densities with different connection configurations (monopolar and bipolar) and types of coagulants (single-coagulant and dual-coagulant). Comparison of the E-HOC process with different connection configurations and types of coagulants for the treatment of WWTP effluent and IBP revealed that organic removal efficiency was higher for the BE-HOC process compared with the ME-HOC process. Energy consumption was lower for the BE-HOC process than for the ME-HOC process generally. In addition, DOC and IBP removal were significantly enhanced in the BE-HOC process with dual-coagulant generation (released from both Al and Fe electrodes). On the one hand, the better removal performance of the BE-HOC process and dual-coagulant mode can be ascribed to the enhanced generation of polymerized Al/Fe species, which improved both the coagulation and catalytic ability of the E-HOC processes. On the other hand, a greater number of active reaction sites of generated hydrolyzed coagulant species was observed in the BE-HOC process and dual-coagulant mode, which led to enhanced •OH generation.

Declaration of Competing Interest

The authors declare that they have no known competing financial interests or personal relationships that could have appeared to influence the work reported in this paper.

Acknowledgments

This work was supported by the National Natural Science Foundation of China (No. 52070151, 51908177), the Key Research and Development Project of Shaanxi Province (2021ZDLSF05–06, 2019ZDLSF05–03), Technology Innovation Leading Program of Shaanxi (2020CGXNG-021) and the New Style Think Tank of Shaanxi Universities.

Supplementary materials

Supplementary material associated with this article can be found, in the online version, at doi:10.1016/j.watres.2021.117600.

References

Abdessamad, N., Akrout, H., Hamdaoui, G., Elghniji, K., Ksibi, M., Bousselmi, L., 2013. Evaluation of the efficiency of monopolar and bipolar BDD electrodes for electrochemical oxidation of anthraquinone textile synthetic effluent for reuse. Chemosphere 93 (7), 1309–1316.

Al-Qodah, Z., Tawalbeh, M., Al-Shannag, M., Al-Anber, Z., Bani-Melhem, K., 2020. Combined electrocoagulation processes as a novel approach for enhanced pollutants removal–A state-of-the-art review. Sci. Total Environ. 744, 140806.

Asselin, M., Drogui, P., Benmoussa, H., Blais, J.F., 2008. Effectiveness of electrocoagulation process in removing organic compounds from slaughterhouse wastewater using monopolar and bipolar electrolytic cells. Chemosphere 72 (11), 1727–1733.

Baes, C.F., Mesmer, R.E., 1976. The Hydrolysis of Cations. Wiley, New York.

Bandaru, S.R.S., Roy, A., Gadgil, A.J., van Genuchten, C.M., 2020. Long-term electrode behavior during treatment of arsenic-contaminated groundwater by a pilot-scale iron electrocoagulation system. Water Res. 175, 115668.

Barazesh, J.M., Hennebel, T., Jasper, J.T., Sedlak, D.L., 2015. Modular advanced oxidation process enabled by cathodic hydrogen peroxide production. Environ. Sci. Technol. 49 (12), 7391–7399.

Barzegar, G., Wu, J., Ghanbari, F., 2019. Enhanced treatment of greywater using electrocoagulation/ozonation–Investigation of process parameters. Process Saf. Environ. Prot. 121, 125–132.
Bicudo, B., van Halem, D., Trikannad, S.A., Ferrero, G., Medema, G., 2021. Low voltage iron electrocoagulation as a tertiary treatment of municipal wastewater–Removal of enteric pathogen indicators and antibiotic-resistant bacteria. Water Res. 188, 116500.
Bilińska, L., Blus, K., Gmurek, M., Ledakowicz, S., 2019. Coupling of electrocoagulation and ozone treatment for textile wastewater reuse. Chem. Eng. Technol. 358, 992–1001.
Bing, J.S., Hu, C., Nie, Y.L., Yang, M., Q, J.H., 2015. Mechanism of catalytic ozonation in Fe_2O_3/Al_2O_3@SBA-15 aqueous suspension for destruction of ibuprofen. Environ. Sci. Technol. 49 (3), 1690–1697.
Bing, J., Hu, C., Zhang, L., 2017. Enhanced mineralization of pharmaceuticals by surface oxidation over mesoporous γ-Ti-Al_2O_3 suspension with ozone. Appl. Catal. B: Environ 202, 118–126.
Carlos, E.B.D., Gabriela, R.-.M., Patricia Balderas, H., Carmen Maria, F.M., Manuel Andrés, R., 2014. Enhanced electrocoagulation–New approaches to improve the electrochemical process. J. Electrochem. Sci. Eng. 4 (4), 285–296.
Chen, M., Dollar, O., Shafer-Peltier, K., Randtke, S., Waseem, S., Peltier, E., 2020. Boron removal by electrocoagulation–Removal mechanism, adsorption models and factors influencing removal. Water Res. 170, 115362.
Chen, W., Li, X., Pan, Z., Ma, S., Li, L., 2016. Synthesis of MnO_x/SBA-15 for Norfloxacin degradation by catalytic ozonation. Sep. Purif. Technol. 173, 99–104.
Cheng, W.P., Yu, R.F., Chen, C.H., Chi, C.H., 2003. Enhanced coagulation on reservoir water by dual inorganic coagulants. Environ. Eng. Sci. 20, 229–235.
Das, P.P., Anweshan, Mondal, P., Sinha, A., Biswas, P., Sarkar, S., Purkait, M.K., 2021. Integrated ozonation assisted electrocoagulation process for the removal of cyanide from steel industry wastewater. Chemosphere 263, 128370.
Ding, Y., Zhou, P., Tang, H., 2016. Visible-light photocatalytic degradation of bisphenol A on $NaBiO_3$ nanosheets in a wide pH range–A synergistic effect between photocatalytic oxidation and chemical oxidation. Chem. Eng. Technol. 291, 149–160.
Dong, G., Ai, Z., Zhang, L., 2014. Total aerobic destruction of azo contaminants with nanoscale zero-valent copper at neutral pH–Promotion effect of in situ generated carbon center radicals. Water Res. 66, 22–30.
Duan, J., Gregory, J., 2003. Coagulation by hydrolyzing metal salts. Adv. Colloid Interface Sci. 100-102, 475–502.
Dubrawski, K.L., van Genuchten, C.M., Delaire, C., Amrose, S.E., Gadgil, A.J., Mohseni, M., 2015. Production and transformation of mixed-valent nanoparticles generated by Fe(0) electrocoagulation. Environ. Sci. Technol. 49 (4), 2171–2179.
Duong, L.V., Wood, B.J., Kloprogge, J.T., 2005. XPS study of basic aluminum sulphate and basic aluminium nitrate. Mater. Lett. 59 (14), 1932–1936.
Feng, G., Cheng, P., Yan, W., Boronat, M., Li, X., Su, J.-.H., Wang, J., Li, Y., Corma, A., Xu, R., Yu, J., 2016. Accelerated crystallization of zeolites via hydroxyl free radicals. Sci. 351 (6278), 1188–1191.
Ghahrchi, M., Rezaee, A., 2020. Electro-catalytic ozonation for improving the biodegradability of mature landfill leachate. J. Environ. Manage. 254, 109811.
Ghahrchi, M., Rezaee, A., 2021. Electrocatalytic ozonation process supplemented by EDTA-Fe complex for improving the mature landfill leachate treatment. Chemosphere 263, 127858.
Ghahrchi, M., Rezaee, A., Adibzadeh, A., 2021. Study of kinetic models of olive oil mill wastewater treatment using electrocoagulation process. Desalin. Water Treat. 211, 123–130.
Ghosh, D., Medhi, C.R., Purkait, M.K., 2008. Treatment of fluoride-containing drinking water by electrocoagulation using monopolar and bipolar electrode connections. Chemosphere 73 (9), 1393–1400.
Golder, A.K., Samanta, A.N., Ray, S., 2007. Removal of Cr^{3+} by electrocoagulation with multiple electrodes–Bipolar and monopolar configurations. J. Hazard. Mater. 141 (3), 653–661.
Harif, T., Khai, M., Adin, A., 2012. Electrocoagulation versus chemical coagulation–Coagulation/flocculation mechanisms and resulting floc characteristics. Water Res. 46 (10), 3177–3188.
Heffron, J., McDermid, B., Maher, E., McNamara, P.J., Mayer, B.K., 2019. Mechanisms of virus mitigation and suitability of bacteriophages as surrogates in drinking water treatment by iron electrocoagulation. Water Res. 163, 114877.
Hellman, H., Laitinen, R.S., Kaila, L., Jalonen, J., Hietapelto, V., Jokela, J., Sarpola, A., Ramo, J., 2006. Identification of hydrolyzis products of $FeCl_3$•$6H_2O$ by ESI-MS. J. Mass Spectrom. 41 (11), 1421–1429.
Hu, C.Z., Wang, S.Q., Sun, J.Q., Liu, H.J., Qu, J.H., 2016. An effective method for improving electrocoagulation process–Optimization of Al_{13} polymer formation. Colloids Surf. A Physicochem. Eng. Asp. 489, 234–240.
Ingelsson, M., Yasri, N., Roberts, E.P.L., 2020. Electrode passivation, faradaic efficiency, and performance enhancement strategies in electrocoagulation–Areview. Water Res. 187, 116433.
Jin, X., Liu, Y., Wang, Y., Zhang, S., Zhang, W., Jin, P., Xu, L., Shi, X., Wang, X.C., Lv, S., 2020a. Towards a comparison between the hybrid ozonation-coagulation (HOC) process using Al- and Fe-based coagulants–Performance and mechanism. Chemosphere 253, 126625.
Jin, X., Wang, Y., Zhang, W., Jin, P., Wang, X.C., Wen, L., 2019. Mechanism of the hybrid ozonation-coagulation (HOC) process–Comparison of preformed Al_{13} polymer and in situ formed Al species. Chemosphere 229, 262–272.
Jin, X., Xie, X., Liu, Y., Wang, Y., Wang, R., Jin, P., Yang, C., Shi, X., Wang, X.C., Xu, H., 2020b. The role of synergistic effects between ozone and coagulants (SOC) in the electro-hybrid ozonation-coagulation process. Water Res. 177, 115800.
Kobya, M., Ulu, F., Gebologlu, U., Demirbas, E., Oncel, M.S., 2011. Treatment of potable water containing low concentration of arsenic with electrocoagulation–Different connection modes and Fe-Al electrodes. Sep. Purif. Technol. 77 (3), 283–293.
Koparal, A.S., Öğütveren, Ü.B., 2002. Removal of nitrate from water by electroreduction and electrocoagulation. J. Hazard. Mater. 89 (1), 83–94.
Lacasa, E., Llanos, J., Cañizares, P., Rodrigo, M.A., 2012. Electrochemical denitrification with chlorides using DSA and BDD anodes. Chem. Eng. Technol. 184, 66–71.
Leveneur, J., Waterhouse, G.I.N., Kennedy, J., Metson, J.B., Mitchell, D.R.G., 2011. Nucleation and growth of Fe nanoparticles in SiO_2: a TEM, XPS, and Fe L-edgexanes investigation. J. Phys. Chem. C 115 (43), 20978–20985.
Li, M., Xia, J., Tian, R., Wang, J., Fan, J., Du, J., Long, S., Song, X., Foley, J.W., Peng, X., 2018. Near-infrared light-initiated molecular superoxide radical generator–Rejuvenating photodynamic therapy against hypoxic tumors. J. Am. Chem. Soc. 140 (44), 14851–14859.
Li, X., Wang, Y., Yuan, S., Li, Z., Wang, B., Huang, J., Dong, S., Yu, G., 2014. Degradation of the anti-inflammatory drug ibuprofen by electro-peroxone process. Water Res. 63, 81–93.
Lin, J.-.L., Chin, C.-J.M., Huang, C., Pan, J.R., Wang, D., 2008. Coagulation behavior of Al_{13} aggregates. Water Res. 42 (16), 4281–4290.
Lin, J.L., Huang, C., Dempsey, B., Hu, J.Y., 2014. Fate of hydrolyzed Al species in humic acid coagulation. Water Res. 56, 314–324.
Ma, M., Liu, R.P., Liu, H.J., Qu, J.H., 2014. Mn(VII)-Fe(II) pre-treatment for Microcystis aeruginosa removal by Al coagulation–Simultaneous enhanced cyanobacterium removal and residual coagulant control. Water Res. 65, 73–84.
Mavré, F., Anand, R.K., Laws, D.R., Chow, K.F., Chang, B.Y., Crooks, J.A., Crooks, R.M., 2010. Bipolar electrodes–A useful tool for concentration, separation, and detection of analytes in microelectrochemical systems. Anal. Chem. 82 (21), 8766–8774.
Mouedhen, G., Feki, M., Wery, M.D., Ayedi, H.F., 2008. Behavior of aluminum electrodes in electrocoagulation process. J. Hazard. Mater. 150 (1), 124–135.
Müller, S., Behrends, T., van Genuchten, C.M., 2019. Sustaining efficient production of aqueous iron during repeated operation of Fe(0)-electrocoagulation. Water Res. 155, 455–464.
Sohlberg, K., Pennycook, S.J., Pantelides, S.T., 1999. Explanation of the observed dearth of three-coordinated Al on γ-alumina surfaces. J. Am. Chem. Soc. 121 (47), 10999–11001.
Tan, C., Dong, Y., Fu, D., Gao, N., Ma, J., Liu, X., 2018. Chloramphenicol removal by zero-valent iron activated peroxymonosulfate system–Kinetics and mechanism of radical generation. Chem. Eng. Technol. 334, 1006–1015.
Tang, H.X., Xiao, F., Wang, D.S., 2015. Speciation, stability, and coagulation mechanisms of hydroxyl aluminum clusters formed by PACl and alum–A critical review. Adv. Colloid Interface Sci. 226, 78–85.
Wang, D., Zhao, Y., Xie, J., Chow, C.W.K., van Leeuwen, J., 2013. Characterizing DOM and removal by enhanced coagulation–A survey with typical Chinese source waters. Sep. Purif. Technol. 110, 188–195.
Xiong, Z., Lai, B., Yang, P., 2018. Insight into a highly efficient electrolysis-ozone process for N, N-dimethylacetamide degradation–Quantitative analysis of the role of catalytic ozonation, Fenton-like and peroxone reactions. Water Res. 140, 12–23.
Xu, W., Gao, B., Yue, Q., Wang, Q., 2011. Effect of preformed and non-preformed Al_{13} species on evolution of floc size, strength and fractal nature of humic acid flocs in coagulation process. Sep. Purif. Technol. 78 (1), 83–90.
Yan, M., Wang, D., Ni, J., Qu, J., Chow, C.W.K., Liu, H., 2008. Mechanism of natural organic matter removal by poly aluminum chloride–Effect of coagulant particle size and hydrolyzis kinetics. Water Res. 42 (13), 3361–3370.
Yu, W.Z., Gregory, J., Graham, N., 2016. Regrowth of broken hydroxide flocs–Effect of added fluoride. Environ. Sci. Technol. 50 (4), 1828–1833.
Zhao, H., Dong, Y., Jiang, P., Wang, G., Zhang, J., Zhang, C., 2015. $ZnAl_2O_4$ as a novel high-surface-area ozonation catalyst–One-step green synthesis, catalytic performance and mechanism. Chem. Eng. Technol. 260, 623–630.
Zhao, H., Liu, H., Qu, J., 2009a. Effect of pH on the aluminum salts hydrolyzis during coagulation process–Formation and decomposition of polymeric aluminum species. J. Colloid Interface Sci. 330 (1), 105–112.
Zhao, L., Sun, Z., Ma, J., 2009b. Novel relationship between hydroxyl radical initiation and surface group of ceramic honeycomb supported metals for the catalytic ozonation of nitrobenzene in aqueous solution. Environ. Sci. Technol. 43 (11), 4157–4163.